Journal of Industrial and Engineering Chemistry 117 (2023) 298–306

Contents lists available at ScienceDirect

Journal of Industrial and Engineering Chemistry

journal homepage: www.elsevier.com/locate/jiec

Random wrinkle structures for spectrum preserved warm white organic light emitting diodes

Jaehyun Moon [a,b,*], Keunsoo Lee [a], Seung Koo Park [a], Chul Woong Joo [a], Jin-Wook Shin [a], Jonghee Lee [a], Jun-Han Han [a], Nam Sung Cho [a]

[a] Reality Devices Research Division, Electronics and Telecommunications Research Institute (ETRI), Daejeon 34129, Republic of Korea
[b] Department of Advanced Device Engineering, University of Science and Technology (UST), Daejeon 34113, Republic of Korea

ARTICLE INFO

Article history:
Received 1 September 2022
Revised 29 September 2022
Accepted 12 October 2022
Available online 19 October 2022

Keywords:
Wrinkles
Surface metrology
White organic light emitting diode
Efficiency
Spectrum
Lighting panel

ABSTRACT

Surface wrinkles of mesoscopic size were formed by a single photocuring process of an in-house synthesized linear liquid pre-polymer. The linear relationship between the amplitude and the period of the wrinkles indicates the presence of constant compressive strain during the wrinkling process. The stiffness ratio of the hard film to the soft foundation decreases as the initial film becomes thinner, providing a quantitative measure for estimating the wrinkle size. As an application, mesoscopic wrinkles were investigated as optical structures for enhanced light outcoupling and angular spectral stability of red, green, blue, and white organic light emitting diodes.

Introduction

Wrinkles are frequently observed in nature [1]. Their size ranges from a nanometric to mountain scale. Wrinkle formation is predominantly a mechanical process, which takes place in systems consisting of a hard skin on a soft foundation [2–5]. Theoretical mechanics studies, processing and applications related to wrinkles have been extensively explored. To induce wrinkle formation numerous strategies have been suggested. One option is a two-material system where the constituents have different Young's moduli [6]. In a single material system, the surface can be selectively treated to form wrinkles [7]. A hard film can be deposited on a pre-stretched mechanically compliant substrate to form wrinkles [8]. A synthesized liquid pre-polymer has also been used to form fine wrinkles [9].

The morphological feature of wrinkles has been probed in various fields. Wrinkle guided microcracks have been used to strain sensors [10]. Corrugated light emitting devices have been fabricated to extract lost photonics modes [11]. Shell type wrinkles have been formed on piezoresistive fibers to enhance the fiber's mechanical response [12]. Because of their stress relaxing capacity, wrinkles have been widely applied in skintronics and e-skin fields, where stretchability and conformal attachment are important [13,14].

In this work, we probed our wrinkle in white organic light emitting diodes (WOLEDs). In OLEDs, while other formats exist, emissive layers of three primary colors of red, green, and blue are used to generate white color or fabricate WOLED [15,16]. Because of the fine thickness of OLED devices, wavelength dependent internal optics is inherently present in OLEDs [17,18]. For this reason, tailoring the internal optics of WOLEDs is not easy [19]. Thus, because the complicated internal optics can be circumvented, external methods have been the preferred method for improved WOLED light out coupling [20]. In this work, we focus on the use of mesoscopic sized wrinkles for WOLEDs to achieve both enhanced light extraction and angular spectral stability. We also demonstrate large area (100 mm × 100 mm) fabrication of wrinkled films and their application to white OLED panels.

Results

Mesoscopic wrinkles

In this section, we investigate structural features of wrinkles. We used a liquid pre-polymer that spontaneously forms wrinkles upon a photo curing process [21]. The initial film is in a liquid state

* Corresponding author at: Reality Devices Research Division, Electronics and Telecommunications Research Institute (ETRI), Daejeon 34129, Republic of Korea.
E-mail address: jmoon@etri.re.kr (J. Moon).

https://doi.org/10.1016/j.jiec.2022.10.018
1226-086X/

and thus is free of strain. During the photo curing process, the upper surface of the pre-polymer cures to become a hard layer. The stiffness difference between the hard surface layer and the soft support leads to the emergence of wrinkles. Geometrically, wrinkle formation on the hard skin is due to the system response to accommodate the imposed strain [22]. An energetic approach has been used to find the relationship between the wavelength and amplitude of the wrinkles [2]. Qualitatively, the wavelength of wrinkle is determined by competition between the upper hard part and the lower soft foundation. Energetically, the former counters short wavelength, while the latter resists long wavelength. We adjusted the spin casting speed to vary the initial thickness of liquid pre-polymer film, and hence, the final wrinkle size. Fig. 1(a) shows the relation between amplitude (A), and period or wavelength (λ). To obtain quantitative values of A and λ, we have performed atomic force microscopy (AFM) scans on wrinkle surfaces. A varies as 200 ∼ 800 nm and λ as 2.4 ∼ 4.8 μm. The inset shows an AFM image of our wrinkles. Quantitative data accompanied with analytical theory offer mechanical characterization of wrinkles. As the theory dictates, there exists a liner relation between the A and λ, i.e.$A = \frac{\sqrt{2}}{\pi}\left(\frac{\Delta}{W}\right)^{1/2}\lambda$. Thus, from the slope, i.e. in the A versus λ space, it is possible to extract the imposed compressive stain (Δ /W) acting on the upper hard part, which is estimated as 0.203. Δ and W refer to displacement and width. The observed linear relation between A and λ strongly indicates that almost an identical compressive strain is present regardless the initial liquid film thickness. Accordingly, a thin initial film gives final wrinkles of smaller size. Fig. 1(b) is a scanning electron microscope (SEM) image of our wrinkles. Close inspections reveal that a few wrinkles are locally aligned to form domains, while long-range ordering is absent. Because we have used bare flat substrates there is no preferred nucleation sites on the surface, resulting in a random distribution of wrinkle domains. The growth direction of wrinkles can be guided by furnishing the substrate with mesa patterns [6]. Domain growth is thought to proceed until adjacent wrinkles are encountered, defining the size of the domain size. Domain size which corresponds to the width of the wrinkle assembly offers a direct clue to estimate the tension along the transverse direction of wrinkles.

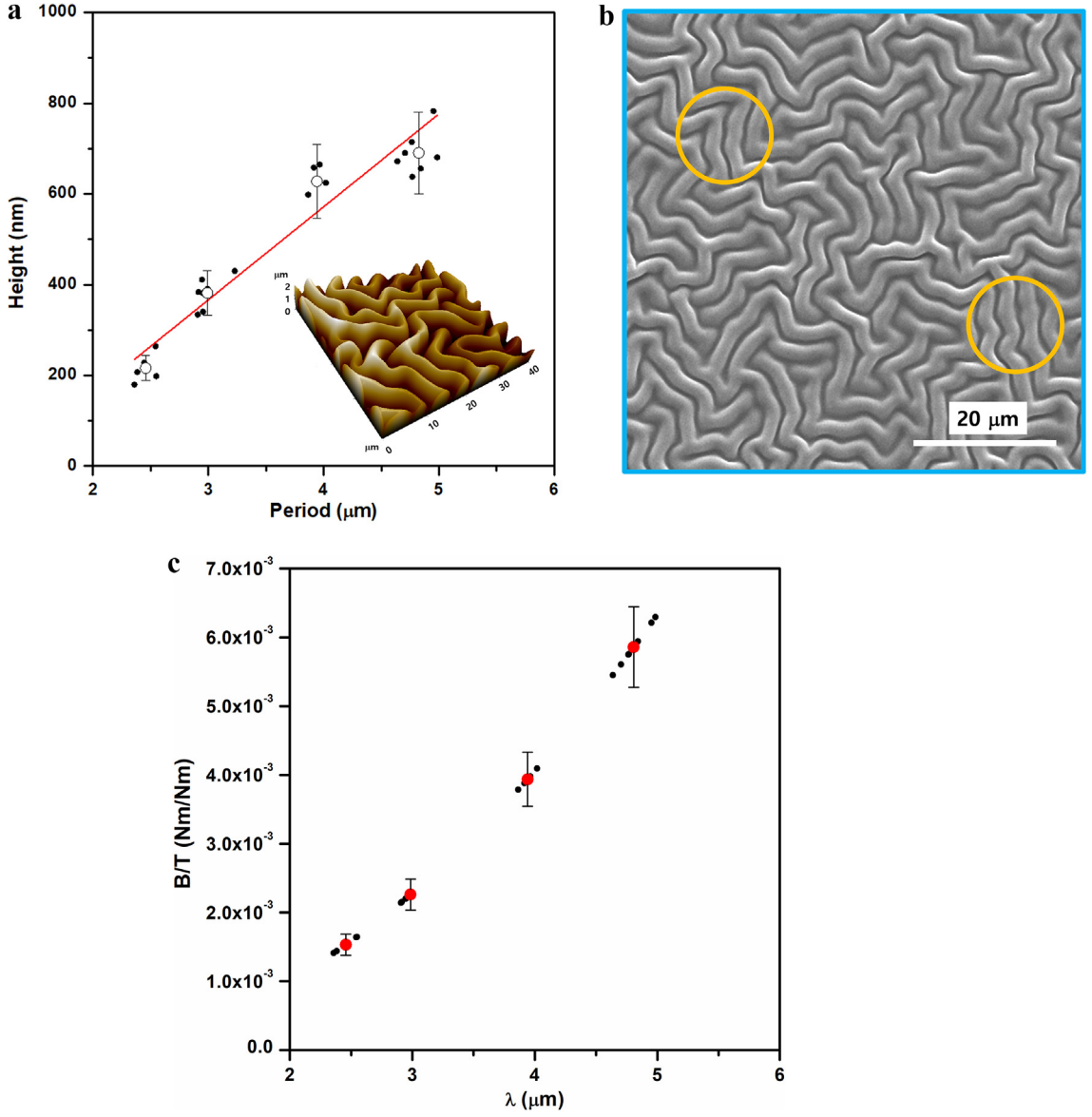

Fig. 1. (a) The relation between height or amplitude (A), and period or wave length (λ) (Inset: An AFM image of wrinkles.), (b) An SEM image of wrinkles highlighting locally aligned wrinkle domains. (c) The stiffness ratio (B/K) of the hard part to the soft hard part as a function of λ.

Using the relation $\lambda = 2\sqrt{\pi}\ (\frac{B}{T})^{1/4} D^{1/2} d$ taking **D** as the domain size, it is possible to estimate the stiffness ratio (**B/T**) of the hard part to the soft hard part. B and T are the bending stiffness of the wrinkle part and stiffness of the foundation, respectively. Using an AFM facility, we have line scanned several domains to extract the size of **D** s. **D** size decreases as the wrinkle size decreases. To be specific **D** varies as 12–24 μm with a corresponding λ of 2.4–4.8 μm. The ratio gradually decreases as λ decreases (Fig. 1(c)). Qualitatively, this indicates that as the initial films become thinner the ratio threshold for wrinkle formation is eased. The approach suggests that size analyses of wrinkles can offer quantitative information, which otherwise is difficult to probe directly.

Fig. 2(a) shows two photographs of wrinkles formed on a flexible substrate of 100 mm × 100 mm. By using our wrinkle forming liquid solution, it is possible to form a wrinkle layer on large area substrates. The wrinkle-bearing films exhibit high haze, indicating wrinkle capacity of deflecting the traveling path of incident light. Fig. 2**(b)** shows a series of SEM images of wrinkles of different size. The size (λ/A) of Wrinkle A, Wrinkle B and Wrinkle C were 4.6 μm/ 800 nm, 3.5 μm/ 530 nm and 2.3 μm/ 250 nm, respectively. As the initial film becomes thinner, A and λ become smaller. But the random distribution does change. To evaluate the wrinkle ability to deflect paths, we measured the transmittance and haze of the wrinkles in Fig. 2(b). The measurement results are shown in Fig. 2**(c)**. The parallel transmittance (P.T., %) gradually increases as the wrinkle size decreases. The haze, which describes the amount of light scattered when light passes through an optical medium, is inversely proportional to the size of the wrinkle. 2.1 section delineates how surface metrology on wrinkle can be used to describe optical properties. The measurement results strongly indicate that the emission characteristics of flat light or photonic sources may be modified by applying our wrinkle structure on the surface. In particular, in the case of planar light sources, the wrinkle may allow enhanced out-coupling at the air/surface by altering the light path toward the escape cone. Approximately 23 % of light is lost at the substrate/air interface due to the total internal reflection [15].

OLED characteristics

Before examining the white light extraction capacity of wrinkles, we focused on monochromatic OLED light sources of red, green and blue. OLEDs were fabricated by a vacuum deposition method on Indium tin oxide(ITO)/glass substrates. A wrinkled film was attached on the exterior surface of the glass. The refractive indices (n ∼ 1.5) of the supporting film and the adhesive match the glass substrate. Details are given in the Method section. Fig. 3 **(a)** shows the angular luminance (L) distribution of the red, green, and blue OLEDs. L was measured under a constant current condition of 2 mA. We tested two wrinkles of different sizes. The smaller wrinkle (W1) has a geometry of λ ∼ 3.9 μm and A ∼ 550 nm. The bigger wrinkle (W2) has a geometry of λ ∼ 5.6 μm and A ∼750 nm. Compared to the L levels of the reference OLED devices, which have a planar glass surface, the L level of those with wrinkled surfaces shows significant L enhancement over the whole angle range. This result indicates the capacity of the wrinkle to lower incident angle of the OLED light component on the substrate/air interface that leads to outcoupling of a large portion of confined light. W2, the bigger wrinkle, provided greater enhancement in L for all colors. We used an integrating sphere to obtain the EQE values (Fig. 3 **(b)**). The EQE increment by using W2 was 48.5 %, 24.5 % and 29 % for red, green and blue, respectively. The highest EQE of 26.3 % was obtained for the green OLED with W2.

Fig. 4 shows the EL spectra of red, green and blue OLEDs as a function of viewing angle. The positions of the main wavelength and the full width at half maximum showed no significant dependency on the viewing angle. Presumably due to the Lambertian nature of reference devices, the EL spectra dependency on the viewing angle (θ) is not apparently high. To gain quantitative information, we analyzed the angular EL spectra further in the following part.

Fig. 5 is the color difference (CD) as a function of θ. To gain quantitative insight into the role of wrinkles on EL spectral characteristics, we have extracted CD. CD is defined as follows.

$$CD\ (\theta) = [(u'(\theta) - u'(0))^2 + (v'(\theta) - v'(0))^2)]^{1/2}$$

CD (θ) gives the quantitative off-set deviations of the CIE 1976 (u', v') coordinates at a given θ from the corresponding coordinate at the forward direction (θ = 0°) [23]. The 1976 Commission Internationale de l'Éclairage coordinates, u' and v', are extracted from the measured angular EL spectra of Fig. 4. In the case of planar OLEDs, the CD (θ) monotonically increases as the θ increases. OLEDs with wrinkles showed saturation of the CD (θ) values as the angle increased. For all colors, the CD (θ) stabilizing effect of W1 and W2 was comparable upto 50^O. However, at a higher angle ($\theta > 60^O$), the W2 showed lower CD values than CD values of W1. By using wrinkle films, it is possible to stabilize the CD (θ) below 0.007, of which chromatic variation may be regarded as unnoticeable to human eyes [24]. The results of Figs. 3, 4 and 5 confirm the capacity of the wrinkles to not only enhance the EQE but also stabilize the CD (θ) of the three primary colors. Our experimental results can be understood from the viewpoint of geometric optics. In a planar OLED case, the outcoupling is low because only light with incident angle lower than θ = 42° can escape the glass/air interface and outcoupled. θ corresponds to the critical angle of interface. Light of θ > 42°, cannot escape the interface due to the total internal reflection. The measured angular luminance distributions (Fig. 3a) show that with the use of wrinkle films, confined light can be extracted upto a viewing angle of approximately 70°. Our results show that wrinkles can deflect the generated light toward the inner part of the escape cone and enable confined light to outcoupled. Conversely speaking, because wrinkle films enable to achieve identical luminance for lower electrical power, our result is also relevant to energy saving.

In the next part, we applied W1 and W2 to WOLEDs. Our white OLEDs have all phosphorescence emitters of red, green and blue. To enhance the relatively weak blue emission, we used two blue layers. Red and green emitters are positioned between the blue layers. Details of the device stack structure are given in the Methods section.

Fig. 6 shows the characteristics of the white OLEDs. L was measured at $\theta = 0^O$. Ref device is a white OLED with a planar glass surface. Fig. 6**(a)** shows the current density (J)/applied voltage (V)/luminance (L) relations. The J-V characteristic show typical OLED electrical behaviors where a rapid J increase or on-set is observed at an applied voltage of approximately 2.3 V. All J/V curves superimpose at V higher than 3.5 V. However, a difference in L level is observed when wrinkle films is attached. The white OLED with W2 showed higher L than that with W1. Accordingly, the current efficiency (CE, Cd/A), the white OLED with W2 showed the highest CE in the whole J range (Fig. 6**(b)**). The CE decreases as the J increase, indicating the presence of roll-off [25].

Fig. 7 **(a)** shows the angular L distributions obtained under constant current (2 mA). Over the whole angular range white OLED with wrinkles showed higher L level than the Ref device. In accordance with the results of Fig. 5, W2 shows better outcoupling. Fig. 7 **(b)** presents the EQE and power efficacy (PE, lm/W) values, which were measured using an integrating sphere. The EQE increased by 29.3 % and 31 % with W1 and W2, respectively. The PE increased by 39.3 % and 42.6 %. Table 1 summarizes the actual EQE values of reference devices and those with W2.

Fig. 8**(a)** shows the normalized EL spectra of the WOLEDs. In the case of the WOLEDs, the viewing angle-dependent EL spectrum is

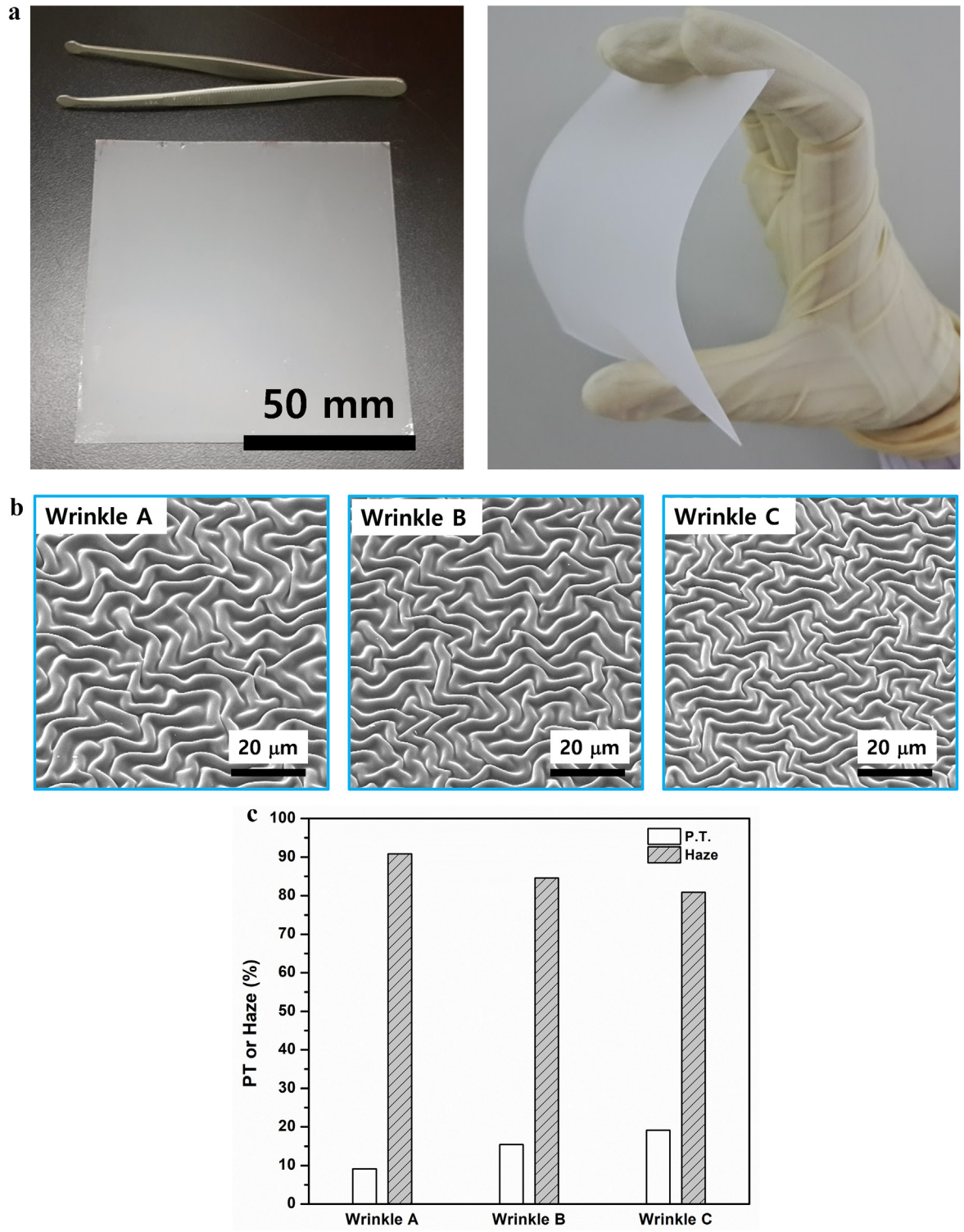

Fig. 2. (a) Photos of wrinkles formed on a flexible substrate of 100 mm × 100 mm. (b) A collection of SEM image of wrinkles with different size. (c) The measured PT and Haze of wrinkles in Fig. 2(b).

due to the wavelength-dependent micro-cavity effect. In other words, as the angle changes the resonance matching wavelength changes, resulting in non-uniform white spectra. Such angle dependency substantially degrades the quality of the planar WOLED light source. The stabilizing effect on the spectra by using wrinkles can be readily observed. This effect is related to the outcoupling function of the wrinkled films as the light outcoupling enhancement of each color is not the same but rather is disproportioned. (Fig. 3). Also, the light extraction is stronger in high angle. These two features are reflected in the angular EL spectra. This feature allows to mixing of photons of each color in various directions of viewing angles to give a rather averaged white emission spectrum. Fig. 7 (b) and (c) present quantitative information. Fig. 8**(b)** is the white angular dependence (WAD). The mathematical definition is identical to CD (θ) and is commonly used to evaluate the angular emission of white light. The WAD increases at

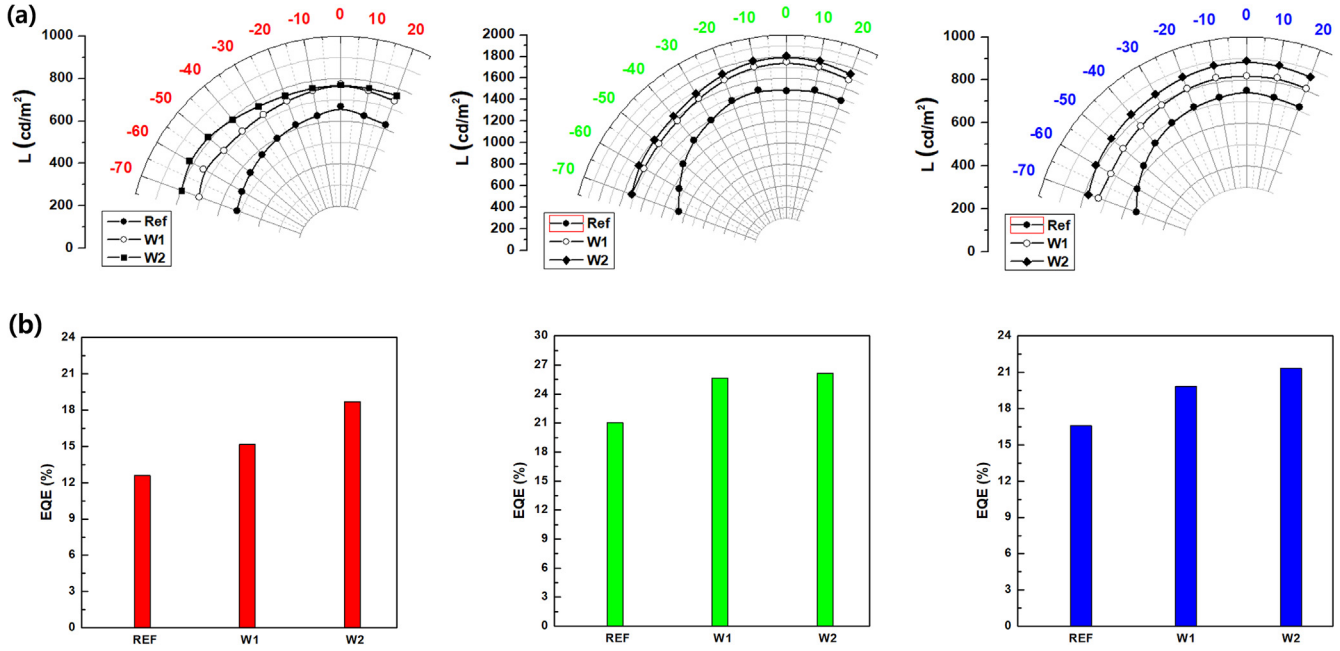

Fig. 3. (a) The angular L distributions and (b) EQE values of red, green and blue OLEDs without (Ref) and with wrinkle films (W1 and W2).

more or less the same rate upto 30°. The WAD gradually flattens but the rate of the white OLED with W2 is a much lower. The largest WAD does not exceed 0.020. The EL spectrum stabilization effect of wrinkle is thought to have its origin in the random distribution, which suppresses the occurrence of preferential emission direction and wavelength. Fig. 7(c) shows the color temperature variation as a function of θ, which was extracted from our white EL spectra in Fig. 8(a) [26]. In all cases, the color temperature gradually increases, indicating stronger blue emission takes place at higher viewing angles. By applying wrinkled films the overall color temperature decreases, making the white light characteristic warmer. This feature is attractive because the eye irritating blue portion is lowered. The color temperature of white OLEDs with W1 and W2 ranges from 2550 to 3090 K and 2650 to 3200 K, respectively. The reference OLED has a range of 2780–3428 K. Recently, the concept of ultrathin emissive layer has been suggested [27]. This approach allows tailoring the emission characteristics in a desired way to fit the application points.

Finally, we applied our white OLED structure and wrinkled films to an IZO (150 nm)/PC (130 μm) flexible substrate to fabricate flexible white OLED light panels. (Fig. 9). On a PC/IZO substrate of 100 mm × 100 mm, three individually operable WOLED panels of 25 mm × 85 mm were fabricated. IZO and PC refer indium zinc oxide and polycarbonate, respectively. IZO was chosen as the transparent electrode due to its mechanical compliance. The apparent emission was uniform over the whole area. Owing to the non-irritating light characteristics, our WOLEDs have wide ranging application possibilities where display units are located in proximity to human eyes. A representative example is AR/VR and the metaverse area. [28]. AR and VR refer to augmented reality and virtual reality.

Methods

Preparation of wrinkles

To form wrinkles, a liquid prepolymer was spin-coated to form an initial liquid thin film. Our prepolymer is an in-house synthesized tetraethylene glycol bis(4-ethenyl-2,3,5,6-tetrafluorophenyl) ether [9]. In the next step, liquid thin film was cross-linked by a UV exposure process, which yields wrinkles [21]. The chemical structure and the schematics of wrinkle preparation process are given in the supporting information (**S1**). Wrinkle films were prepared on polyethylene (PET) films, which have a glass index matching adhesive on one side. To vary the initial film thickness, we varied the spin-coating speed as 2000 rpm, 3000 rpm and 4000 rpm. rpm refers to revolutions per minute. Prior to the coating process, samples were placed at rest for 10 s to obtain a stable well-defined meniscus. UV exposure processes were carried out in an N_2 atmosphere. The exposure time was 10 m. Structural characterizations of wrinkles were performed using scanning electron microscopy (SEM, FEI, Sirion 400) and atomic force microscopy (AFM, XE-100, Park System).

Fabrication of OLEDs

Red, green and blue OLEDs were fabricated on ITO (70 nm)/glass(0.7 mm) substrates using a vacuum evaporation process. All organic layers were deposited in a high vacuum below 6.67×10^{-5} Pa by a thermal evaporation method. The emission area was 10 mm × 7 mm. Red, green and blue OLEDs commonly have Hat-CN(10 nm)/TAPC(50 nm) and BmPyPB(60 nm) as their hole and electron transport layers, respectively. The emitting layers of red, green, and blue were host/dopants types composed of DCzppy:IrMDQ2(acac) (20 nm, 7 %), DCzPPY:Irppy3 (20 nm, 7 %) and DCzppy:FIrpic (20 nm, 7 %), respectively. The cathode was LiF/Al (100 nm. Our phosphorescent white OLEDs have a stack structure of ITO (70 nm)/ Hat-CN (5 nm)/ TAPC (50 nm)/ Hat-CN (10 nm)/ TAPC (50 nm)/ Hat-CN (10 nm)/ TAPC (50 nm)/ TcTa:FIrpic(7 %) (5 nm)/ TcTa:IrMDQ2acac(5 %) (0.5 nm)/TcTa:Irppy3(7 %) (1 nm)/ DCzPPy:Firpic(10 %) (5 nm)/ BmPyPB (55 nm)/ LiF (1 nm)/ Al(100 nm). We used dual layers of blue, TcTa:FIrpic and DCzPPy:Firpic, to augment the relatively weak blue luminance. For the hole transport layer (HTL), we adopted a layered HTL comprising Hat-CN and TAPC, which has been shown to enhance the hole transport and electrically stabilize the device [29]. The full

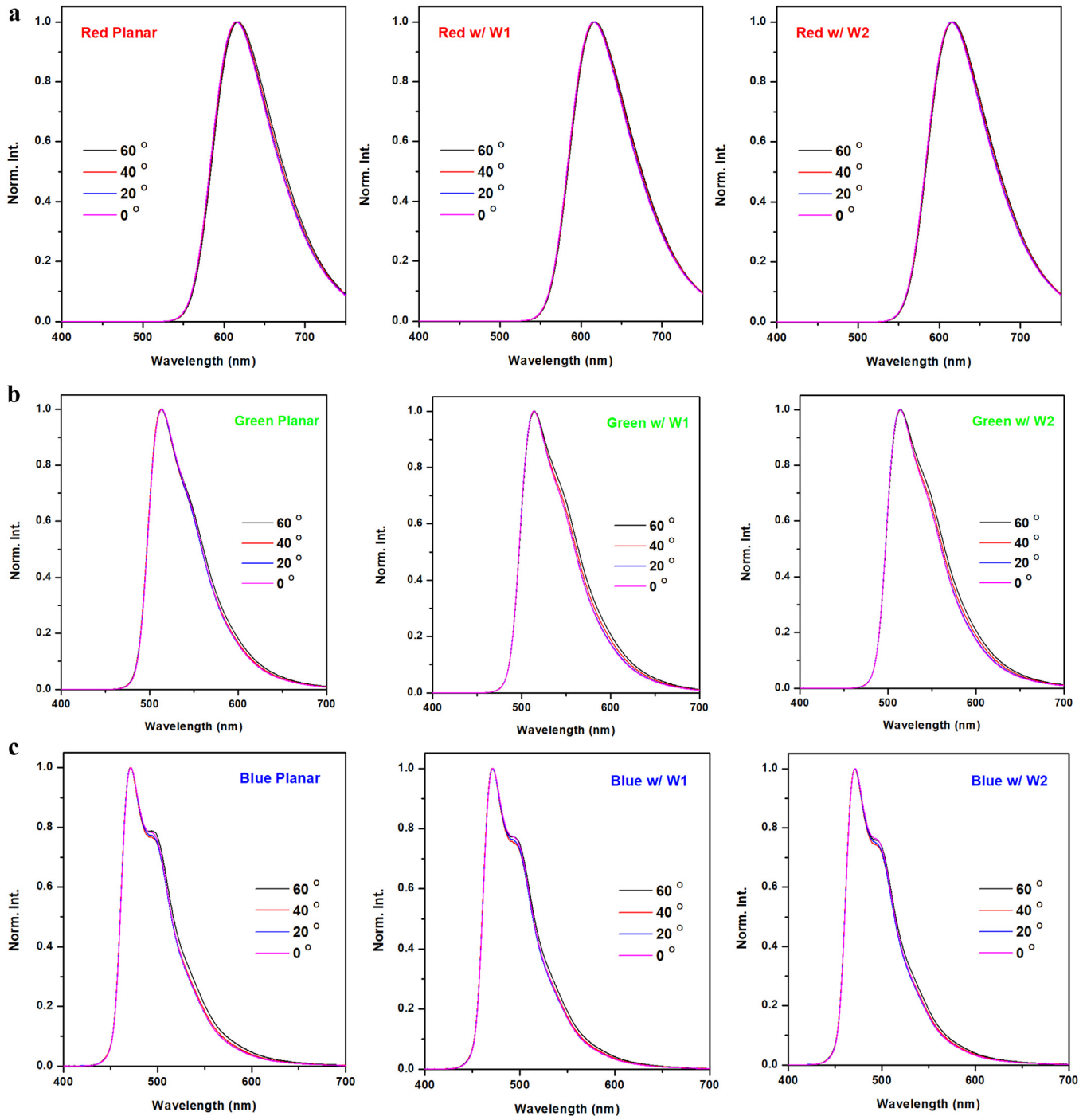

Fig. 4. The EL spectra of (a) red, (b) green and (c) blue OLEDs as a function of viewing angle.

names of the organics and an energy level diagram of our WOLED are summarized in the supplementary information (**S2**). **S3** is an actual photograph of our OLED devices. Also the energy level diagram of our white OLED is shown.

Characterization and measurements

Electroluminescence (EL) spectra were measured with a goniometer-equipped spectroradiometer (Minolta CS-200) and a current–voltage source meter (Keithley 238). The EQE (%) and PE (lm/W) values were measured using an integrating sphere.

Summary

In this work, we introduced mesopic surface wrinkles that were formed by a single photocuring step of a liquid prepolymer. Image analyses and continuum theory were applied to elucidate the A/λ relation of wrinkles and their mechanical characteristics. A and λ revealed a linear relation with a constant imposed compressive stain of 0.203, which is independent of the initial film thickness. The stiffness ratio (B/T) of the hard part to the soft hard part was found to be linearly dependent on the λ of the wrinkles. With the actual λ values of the wrinkles it is possible to estimate the

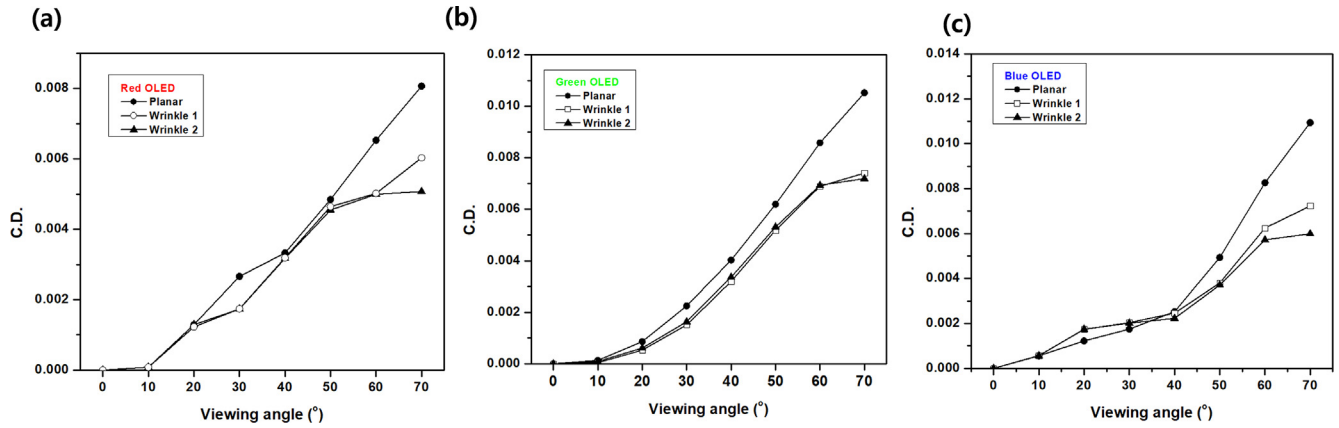

Fig. 5. The CDs of (a) red, (b) green and (c) blue OLEDs as a function of viewing angle.

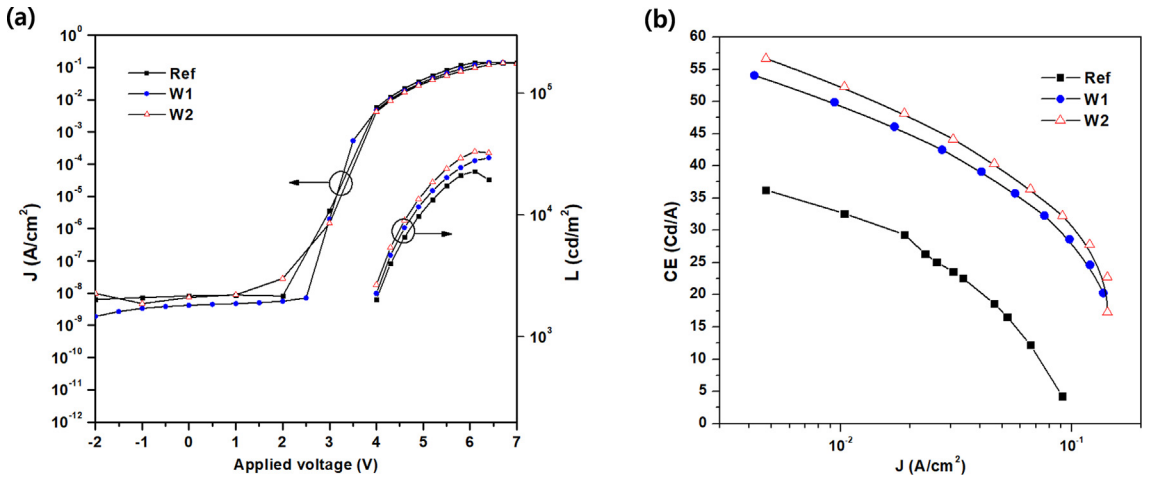

Fig. 6. (a) The current density (J)/applied voltage (V)/luminance (L) relations and (b) The current efficiency (CE, Cd/A) of white OLEDs without (Ref) and with wrinkle films (W1 and W2).

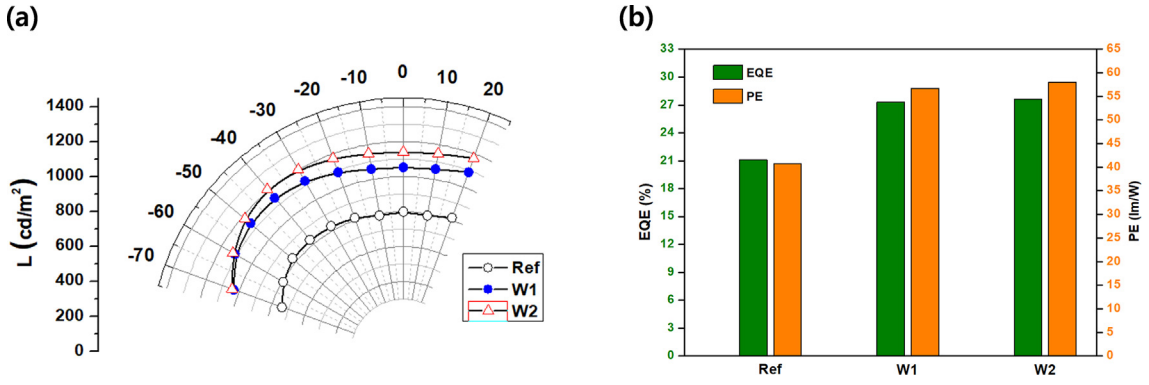

Fig. 7. (a) The angular L distributions and (b) the EQE and PE values of white OLEDs without (Ref) and with wrinkle films (W1 and W2).

Table 1
EQE values and corresponding increment by using wrinkles on OLEDs.

	EQE (%)		Increment (%)
	Ref	w/ W2	
Red	12.59	18.70	48.5
Green	21.03	26.15	24.5
Blue	16.57	21.33	29
White	21.1	27.6	31

B/T, or conversely the estimate wrinkle sizes. The presented analyses can be extended to various wrinkling and buckling systems to estimate the relative strain, which is normally difficult to gauge. To explore the application aspects of wrinkles, we applied our wrinkled film as an optical functional for achieving enhanced efficiency and spectral stability of red, green, blue, and white OLEDs. The EQE increment by using wrinkles was 48.5 %, 24.5 %, 29 % and 31 % for red, green, blue and white, respectively. By using wrinkles, the measured angular EL spectrum chromatic variations

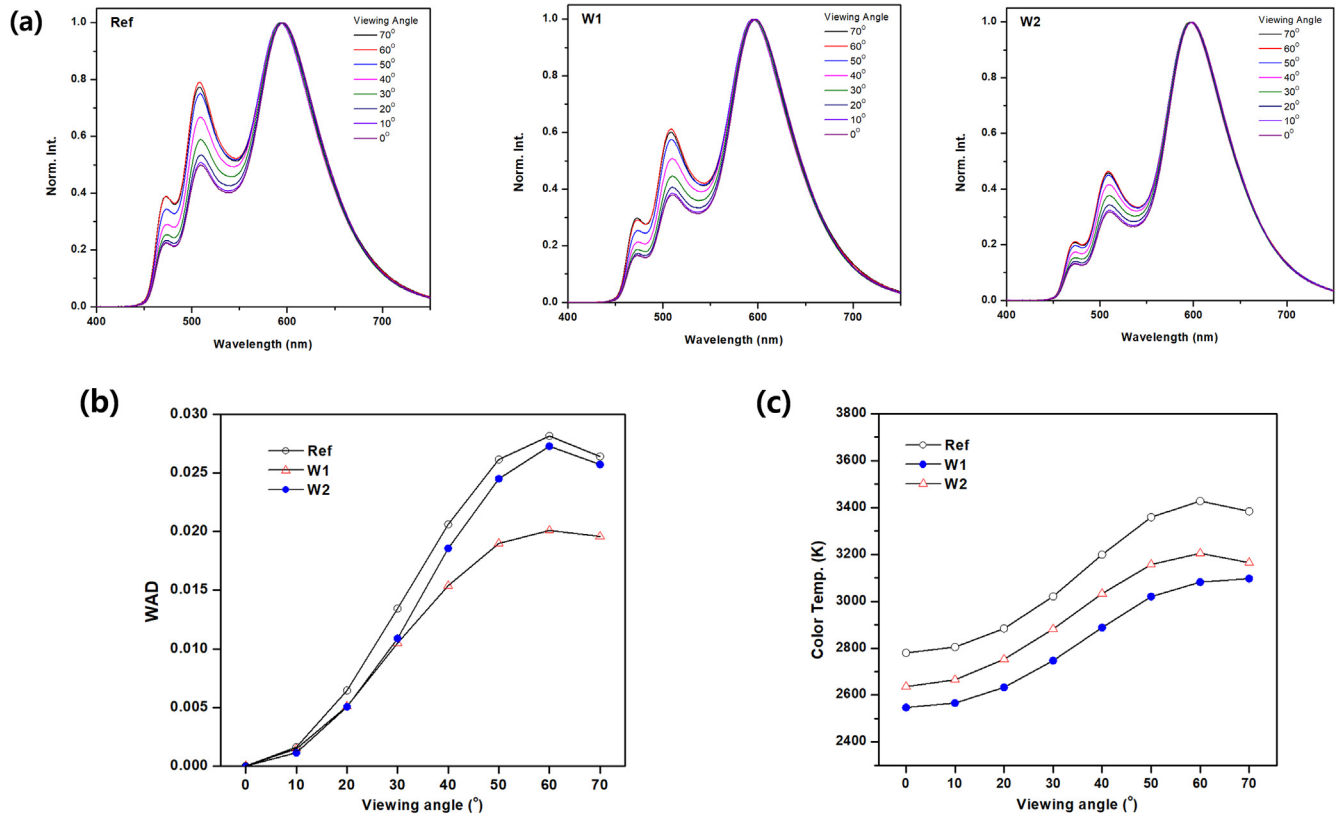

Fig. 8. (a) The EL spectra of white OLEDs as a function of viewing angle. (b) The WAD and (c) the color temperature of white OLEDs as a function of viewing angle.

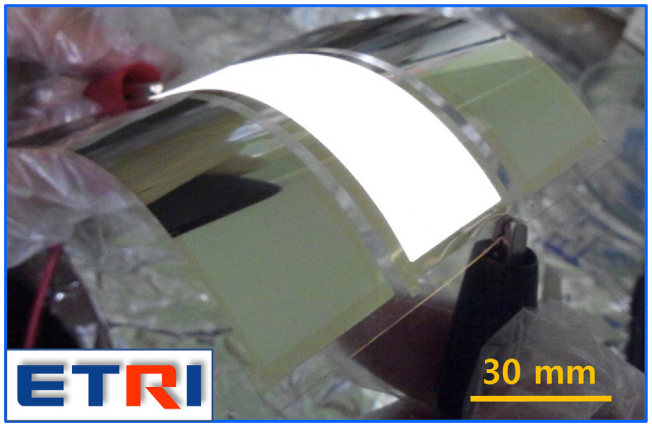

Fig. 9. A flexible white OLED light panel with of three 25 mm × 85 mm lighting units.

or WAD were unnoticeable to the human eye for all colors. We attribute this beneficial effect to the random distribution and the suitable mesopic size of wrinkles. We believe that our approach has wide-ranging applications where physical lightness, a human eye-friendly light source and form factor are important.

Declaration of Competing Interest

The authors declare that they have no known competing financial interests or personal relationships that could have appeared to influence the work reported in this paper.

Acknowledgements

This work was supported by Electronics and Telecommunications Research Institute (ETRI) grant funded by the Korean government (22ZB1200).

Appendix A. Supplementary data

Supplementary data to this article can be found online at https://doi.org/10.1016/j.jiec.2022.10.018.

References

[1] B. Li, Y.-P. Cao, X.-Q. Feng, H. Gao, Soft Matter 2012 (8) (2018) 5728–5745, https://doi.org/10.1039/C2SM00011C.
[2] E. Cerda, L. Mahadevan, Phys. Rev. Lett. 90 (2003), https://doi.org/10.1103/PhysRevLett.90.074302.
[3] H. Jiang, D.-Y. Khang, J. Song, Y. Sun, Y. Huang, J. Rogers, Proc. Natl. Acad. Sci. U. S.A. 104 (2007) 15607–156122, https://doi.org/10.1073/pnas.0702927104.
[4] Z. Huang, W. Hong, Z. Suo, Phys. Rev. E 70 (2004), https://doi.org/10.1103/PhysRevE.70.030601, 030601(R).
[5] J. Rodríguez-Hernández, Prog. Polymer Sci. 42 (2015) 1–41, https://doi.org/10.1016/j.progpolymsci.2014.07.008.
[6] N. Bowden, S. Brittain, A. Evans, J. Hutchinson, G. Whitesides, Nature 393 (1998) 146–149, https://doi.org/10.1038/30193.
[7] D. Chandra, A. Crosby, Adv. Mater. 23 (2011) 3441–3445, https://doi.org/10.1002/adma.201101366.
[8] W.M. Choi, J. Song, D.-Y. Khang, H. Jiang, Y. Huang, J. Rogers, Nano Lett. 7 (2007) 1655–1663, https://doi.org/10.1021/nl0706244.
[9] S.K. Park, Y.-J. Kwark, J. Moon, C.W. Joo, B. Yu, J.-I. Lee, Macromol. Rapid Commun. 2015 (36) (2015) 2006–2011, https://doi.org/10.1002/marc.201500370.
[10] L. Li, Y. Zheng, E. Liu, X. Zhao, S. Yu, J. Wang, et al., Chem. Eng. J. 437 (2022), https://doi.org/10.1016/j.cej.2022.135399.
[11] H. Liang, H.-C. Hsu, J. Wu, X. He, M. Wei, T.-L. Chiu, et al., Opt. Exp. 27 (2019) A372–A384, https://doi.org/10.1364/OE.27.00A372.
[12] Y. Wei, S. Chen, X. Yuan, P. Wang, L. Liu, Adv. Funct. Mater. 26 (2016) 5078–5085, https://doi.org/10.1002/adfm.201600580.

[13] J.J. Kim, Y. Wang, H. Wang, S. Lee, T. Yokota, T. Someya, Adv. Funct. Mater. 31 (39) (2021), https://doi.org/10.1002/adfm.202009602, 2009602.
[14] D. Ge, A. Babangida, Z. Hu, L. Zhang, M. Wang, IEEE Sensors J. 22 (2022) 3040–3051, https://doi.org/10.1109/JSEN.2021.3130445.
[15] S. Reineke, M. Thomschke, B. Lüssem, K. Leo, Rev. Mod. Phys. 85 (2013) 1245–1293, https://doi.org/10.1103/RevModPhys.85.1245.
[16] J. Chen, F. Zhao, D. Ma, Mater. Today 17 (2014) 175–183, https://doi.org/10.1016/j.mattod.2014.04.002.
[17] M. Furno, R. Meerheim, S. Hofmann, B. Lüssem, K. Leo, Phys. Rev. B 85 (2012), https://doi.org/10.1103/PhysRevB.85.115205.
[18] Y. Li, N. Kotadiya, B. Zee, P. Blom, G.-J. Wetzelaer, Adv. Optical Mater. 9 (2021) 2001812, https://doi.org/10.1002/adom.202001812.
[19] H. Cho, J. Song, B.-H. Kwon, S. Choi, H. Lee, C.W. Joo, et al., J. Ind. Eng. Chem. 69 (2019) 414–421, https://doi.org/10.1016/j.jiec.2018.10.006.
[20] H.J. Peng, Y.L. Ho, C.F. Qiu, M. Wong, H.S. Kwok, SID Sym. Digest of Tech. Papers 35 (2004) 158–161, https://doi.org/10.1889/1.1825995.
[21] J.C. Jeong, K.Y. Woo, H. Cho, Y.-H. Cho, N.S. Cho, S.Y. Yang, et al., J. Ind. Eng. Chem. 96 (2021) 163–168, https://doi.org/10.1016/j.jiec.2021.01.025.
[22] L. Ma, L. He, Y. Ni, J. Appl. Phys. 127 (11) (2020), https://doi.org/10.1063/1.5143651, 111101.
[23] E. Kim, J. Chung, J. Lee, H. Cho, N.S. Cho, S. Yoo, Org. Elec. 48 (2017) 348–356, https://doi.org/10.1016/j.orgel.2017.06.030.
[24] T. Komoda, H. Tsuji, K. Yamae, K. Varutt, Y. Matsuhisa, N. Ide, SID Sym. Digest of Tech. Papers 42 (2011) 1056–1059, https://doi.org/10.1889/1.3621004.
[25] C. Murawski, K. Leo, M. Gather, Adv. Mater. 25 (2013) 6801–6827, https://doi.org/10.1002/adma.201301603.
[26] C.W. Joo, J. Moon, J.-H. Han, J.W. Huh, J. Lee, N.S. Cho, et al., Org. Elec. 15 (2014) 189–195, https://doi.org/10.1016/j.orgel.2013.10.005.
[27] Y. Miao, M. Yin, iScience 25 (2022), https://doi.org/10.1016/j.isci.2022.103804.
[28] H. Cho, C.W. Joo, S. Choi, C.-M. Kang, G.H. Kim, J.-W. Shin, et al., ETRI J. 4 (2021) 1093–1102, https://doi.org/10.4218/etrij.2020-0321.
[29] J. Moon, J.-W. Shin, H. Cho, J.-H. Han, N.S. Cho, J.T. Lim, et al., Diam. Relat. Mater. 57 (2015) 68–73.